ACS APPLIED MATERIALS & INTERFACES

Research Article

www.acsami.org

# Bis(thienothiophenyl) Diketopyrrolopyrrole-Based Conjugated Polymers with Various Branched Alkyl Side Chains and Their Applications in Thin-Film Transistors and Polymer Solar Cells

Jicheol Shin, Gi Eun Park, Dae Hee Lee, Hyun Ah Um, Tae Wan Lee, Min Ju Cho, and Dong Hoon Choi*

Department of Chemistry, Research Institute for Natural Sciences, Korea University, 5 Anam-dong, Sungbuk-gu, Seoul 136-701, Korea

Supporting Information

**ABSTRACT:** New thienothiophene-flanked diketopyrrolopyrrole and thiophene-containing $\pi$-extended conjugated polymers with various branched alkyl side-chains were successfully synthesized. 2-Octyldodecyl, 2-decyltetradecyl, 2-tetradecylhexadecyl, 2-hexadecyloctadecyl, and 2-octadecyldocosyl groups were selected as the side-chain moieties and were anchored to the N-positions of the thienothiophene-flanked diketopyrrolopyrrole unit. All five polymers were found to be soluble owing to the bulkiness of the side chains. The thin-film transistor based on the 2-tetradecylhexadecyl-substituted polymer showed the highest hole mobility of 1.92 $cm^2\ V^{-1}\ s^{-1}$ due to it having the smallest $\pi-\pi$ stacking distance between the polymer chains, which was determined by grazing incidence X-ray diffraction. Bulk heterojunction polymer solar cells incorporating [6,6]-phenyl-C71-butyric acid methyl ester as the n-type molecule and the additive 1,8-diiodooctane (1 vol %) were also constructed from the synthesized polymers without thermal annealing; the device containing the 2-octyldodecyl-substituted polymer exhibited the highest power conversion efficiency of 5.8%. Although all the polymers showed similar physical properties, their device performance was clearly influenced by the sizes of the branched alkyl side-chain groups.

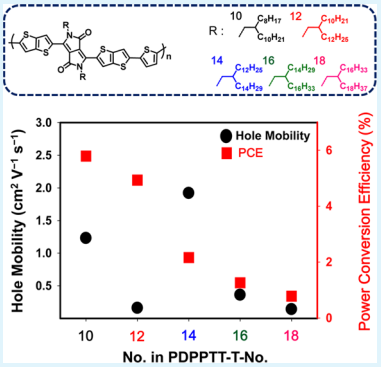


**KEYWORDS:** *polymer semiconductor, diketopyrrolopyrrole, branched alkyl side chain, thin-film transistor, polymer solar cell*

## INTRODUCTION

Solution-processable conjugated polymers have attracted considerable attention due to their applicability in thin-film transistors (TFTs) and polymer solar cells (PSCs).[1−3] They are well-suited for the fabrication of large-scale devices via spin coating, dip coating, screen printing, and drop casting, although they do require specific solvents that are precisely selected to control thin-film crystallinity and polymer chain arrangement on substrates. Most recently, outstanding TFT device performance has been observed in soluble donor−acceptor (D−A) alternating conjugated polymers in which the donors, acceptors, side-chains, and conjugation length have been fully optimized.[4,5] The alkyl side chains tethered to the polymer backbone are in particular one of the most important of these factors; properly selecting tethering position and size, in providing the appropriate length and bulkiness, directly controls crystallinity in the solid state and solubility in organic solvents. Many previous reports show that bulkiness helps to control the interaction between the polymer chains and to modulate the lamella and $\pi-\pi$ stacking distances, which in turn can affect physical properties and corresponding device performance.[6−10]

Linear alkyl side chains were introduced to help solubilize conjugated polymers at the very beginning of polymer-based electronics and optoelectronics research. However, several $\pi$-extended D−A conjugated copolymers exhibited poor solubility in common organic solvents when linear alkyl side chains were used, due not only to the strong intermolecular interactions caused by extended delocalization but also to possible interdigitation of the linear side chains as well.[11−14] Fortunately, branched alkyl side chains have been shown to suppress intermolecular interaction, resulting in improved solubility;[15,16] this modification has been used in the development of multiple copolymers with high device performance that had been optimized by changing branched alkyl side-chain length and branching point.[17−22] However, despite the importance of this innovation, a systematic study on the effects of the bulkiness of branched alkyl side chains has not been completed previously.

In this work, we synthesized a series of thienothiophene-flanked diketopyrrolopyrrole (DPPTT)-based copolymers with 2-octyldodecyl,[23,24] 2-decyltetradecyl,[25] 2-tetradecylhexadecyl, 2-hexadecyloctadecyl, and 2-octadecyldocosyl branched side chains to investigate these effects, focusing especially on device performance. Polymer crystallinity and morphology were investigated through grazing incidence X-ray diffraction (GI-

Received: November 16, 2014
Accepted: January 15, 2015
Published: January 15, 2015





DOI: 10.1021/am508026s
ACS Appl. Mater. Interfaces 2015, 7, 3280−3288

XRD) and atomic force microscopy (AFM). Although each film showed similar absorption and electrochemical behavior, their device performances were quite different. Specifically, the 2-tetradecylhexadecyl TFT exhibited the highest hole mobility of 1.92 $cm^2 V^{-1} s^{-1}$, while the blended film combining the 2-octyldodecyl polymer and [6,6]-phenyl-C71-butyric acid methyl ester ($PC_{71}BM$) gave power conversion efficiency (PCE) of 5.8% in PSCs.

## EXPERIMENTAL SECTION

**Materials and Synthesis.** All reagents for preparing the five polymers were purchased from Sigma-Aldrich, TCI (SEJINCI), and Acros Organics and used as received without any more purification. Reagent-grade solvents were purified by a Solvent Dispensing System (J. C. Meyer, Laguna Beach, CA, U.S.A.). Compounds **11**, **12**, and **16** were synthesized following modified literature methods.[23−26] The same applies to **PDPPTT-T-10** and **PDPPTT-T-12** as well.[23−25]

*Synthesis of Compound* ***1***. Potassium hydroxide (200 mg, 0.004 mol) and nickel powder (60 mg, 0.001 mol) were mixed in hexadecan-1-ol (15 g, 0.062 mol). The mixed suspension was stirred at 250 °C for 2 h with a Dean−Stark trap to remove water produced during the reaction. The hot viscous solution was then cooled to room temperature. The concentrated crude solution was purified using column chromatography (eluent = hexane/ethyl acetate, 8:1 v/v) on silica gel to obtain compound **1** as a colorless oil with a yield of 85%. $^1$H NMR (400 MHz, $CDCl_3$) $\delta$ (ppm): 3.54 (d, $J$ = 4.0 Hz, 2H), 1.63 (m, 1H), 1.43−1.09 (m, 56H), 0.88 (m, 6H). $^{13}$C NMR (100 MHz, $CDCl_3$) $\delta$ (ppm): 65.94, 40.73, 32.14, 32.10, 31.12, 30.28, 30.14, 29.91, 29.87, 29.58, 29.53, 27.10, 22.91, 22.89, 17.12, 14.33. Anal. Calcd for $C_{32}H_{66}O$: C, 82.32; H, 14.25. Found: C, 82.46; H, 14.20%.

*Synthesis of Compound* ***2***. Compound **2** was obtained by following a procedure similar to that for compound **1** but by starting from octadecan-1-ol (15 g, 0.055 mol). Compound **2** was obtained as a colorless oil with a yield of 73%. $^1$H NMR (400 MHz, $CDCl_3$) $\delta$ (ppm): 3.54 (d, $J$ = 4.0 Hz, 2H), 1.63 (m, 1H), 1.45−1.06 (m, 64H), 0.88 (m, 6H). $^{13}$C NMR (100 MHz, $CDCl_3$) $\delta$ (ppm): 65.94, 40.74, 32.14, 32.10, 31.11, 30.28, 30.14, 29.98, 29.94, 29.91, 29.87, 29.82, 29.78, 29.58, 29.53, 27.10, 26.68, 22.91, 22.89, 17.12, 14.33. Anal. Calcd for $C_{36}H_{74}O$: C, 82.68; H, 14.26. Found: C, 82.63; H, 14.30%.

*Synthesis of Compound* ***3***. Compound **1** (10 g, 0.021 mol), imidazole (1.76 g, 0.026 mol), and triphenylphosphine (6.82 g, 0.026 mol) were dissolved in methylene chloride (MC, 250 mL), and the mixture was cooled to 0 °C. After iodine (6.60 g, 0.026 mol) was added, the mixture was allowed to stir for 15 min at 0 °C. The reaction temperature was raised to room temperature, and the mixture was kept under stirring overnight. After quenching the reaction mixture with sodium metabisulfite, the MC phase was washed with water and saturated brine a few times, after which it was dried over sodium sulfate. The filtrate was then isolated, and the solvent was evaporated to yield the crude product, which was purified by silica-gel column chromatography (eluent = hexane) to obtain compound **3** as a colorless oil with a yield of 88%. $^1$H NMR (400 MHz, $CDCl_3$) $\delta$ (ppm): 3.27 (d, $J$ = 4.0 Hz, 2H), 1.55 (m, 1H), 1.44−1.10 (m, 56H), 0.88 (m, 6H). $^{13}$C NMR (100 MHz, $CDCl_3$) $\delta$ (ppm): 38.88, 34.61, 32.15, 32.11, 29.93, 29.90, 29.89, 29.85, 29.81, 29.59, 29.55, 26.71, 22.92, 22.88, 17.13, 14.34. Anal. Calcd for $C_{32}H_{65}I$: C, 66.64; H, 11.36. Found: C, 66.71; H, 11.32%.

*Synthesis of Compound* ***4***. Compound **4** was obtained by following a similar procedure as that for compound **3** but by starting from compound **2** (10 g, 0.019 mol). Compound **4** was obtained as a colorless oil with a yield of 83%. $^1$H NMR (400 MHz, $CDCl_3$) $\delta$ (ppm): 3.27 (d, $J$ = 4.0 Hz, 2H), 1.54 (m, 1H), 1.48−1.05 (m, 64H), 0.88 (m, 6H). $^{13}$C NMR (100 MHz, $CDCl_3$) $\delta$ (ppm): 38.88, 34.61, 32.15, 32.11, 31.09, 30.15, 30.03, 29.98, 29.95, 29.90, 29.86, 29.82, 29.79, 29.56, 29.54, 26.75, 26.66, 22.90, 22.88, 17.12, 14.33, 14.31. Anal. Calcd for $C_{36}H_{73}I$: C, 68.32; H, 11.63. Found: C, 68.35; H, 11.62%.

*Synthesis of Compound* ***8***. 13-(Iodomethyl)heptacosane (6.3 g, 10.8 mmol) was added to a mixture of compound **5** (1.5 g, 3.62 mmol) and potassium carbonate (1.8 g, 12.7 mmol) in dry dimethylformamide (50 mL) at 120 °C. After the reaction mixture was kept for 5 h, it was cooled, poured into ice water, and extracted with chloroform. The combined extracts were washed with water and brine and dried over sodium sulfate. The filtrate was then isolated, and the solvent was evaporated to yield the crude product, which was purified by column chromatography (eluent = MC/hexane, 3:1 v/v) on silica gel to obtain compound **8** with a yield of 43%. $^1$H NMR (400 MHz, $CDCl_3$) $\delta$ (ppm): 9.29 (s, 2H), 7.61 (d, $J$ = 8.0 Hz, 2H), 7.32 (d, $J$ = 4.0 Hz, 2H), 4.09 (d, $J$ = 12.0 Hz, 4H), 1.99 (m, 2H), 1.43−1.09 (m, 96H), 0.88 (m, 12H). $^{13}$C NMR (100 MHz, $CDCl_3$) $\delta$ (ppm): 161.72, 143.22, 140.46, 140.29, 132.03, 131.30, 127.49, 120.14, 46.56, 37.22, 31.94, 31.20, 30.05, 29.71, 29.68, 29.59, 29.38, 26.23, 22.71, 14.15. Anal. Calcd for $C_{74}H_{120}N_2O_2S_4$: C, 74.19; H, 10.10; N, 2.34; S, 10.71. Found: C, 74.23; H, 10.05; N, 2.38; S, 10.62%.

*Synthesis of Compound* ***9***. Compound **9** was obtained by following a similar procedure as that for compound **8** but by starting from compound **5** (1.5 g, 3.62 mmol). Compound **9** was obtained as a dark purple solid with a yield of 38%. $^1$H NMR (400 MHz, $CDCl_3$) $\delta$ (ppm): 9.29 (s, 2H), 7.61 (d, $J$ = 8.0 Hz, 2H), 7.32 (d, $J$ = 4.0 Hz, 2H), 4.09 (d, $J$ = 12.0 Hz, 4H), 1.99 (m, 2H), 1.48−1.04 (m, 112H), 0.88 (m, 12H). $^{13}$C NMR (100 MHz, $CDCl_3$) $\delta$ (ppm): 161.74, 143.25, 140.49, 140.30, 132.02, 131.33, 127.51, 120.11, 46.58, 37.35, 31.91, 31.19, 29.95, 29.91, 29.88, 29.85, 29.81, 29.57, 29.33, 26.24, 22.84, 22.68, 17.02, 14.15. Anal. Calcd for $C_{82}H_{136}N_2O_2S_4$: C, 75.17; H, 10.46; N, 2.14; S, 9.79. Found: C, 75.10; H, 10.42; N, 2.09; S, 9.73.

*Synthesis of Compound* ***10***. Compound **10** was obtained by following a similar procedure as that for compound **8** but by starting from compound **5** (1.5 g, 3.62 mmol). Compound **10** was obtained as a dark purple solid with a yield of 41%. $^1$H NMR (400 MHz, $CDCl_3$) $\delta$ (ppm): 9.29 (s, 2H), 7.61 (d, $J$ = 8.0 Hz, 2H), 7.32 (d, $J$ = 4.0 Hz, 2H), 4.09 (d, $J$ = 12.0 Hz, 4H), 1.99 (m, 2H), 1.48−0.98 (m, 128H), 0.88 (m, 12H). $^{13}$C NMR (100 MHz, $CDCl_3$) $\delta$ (ppm): 161.74, 143.32, 140.41, 140.26, 132.07, 131.32, 127.50, 120.12, 46.56, 37.50, 31.90, 31.88, 31.04, 30.14, 30.00, 29.97, 29.95, 29.90, 29.86, 29.59, 29.48, 29.45, 29.38, 26.47, 26.02, 22.76, 22.73, 17.01, 14.26, 14.15. Anal. Calcd for $C_{90}H_{152}N_2O_2S_4$: C, 75.99; H, 10.77; N, 1.97; S, 9.02. Found: C, 76.07; H, 10.84; N, 1.88; S, 8.96%.

*Synthesis of Compound* ***13***. *N*-Bromosuccinimide (0.13 g, 0.72 mmol) was added slowly to a stirred solution of compound **8** (0.4 g, 0.33 mmol) in chloroform (30 mL) under argon, which was then allowed to stir at room temperature overnight. The resulting mixture was extracted with chloroform, after which the combined extracts were washed with water and saturated brine and dried over sodium sulfate. The filtrate was then isolated, and the solvent was evaporated to yield the crude product, which was further purified by column chromatography (eluent = MC/hexane, 4:1 v/v) on silica gel to obtain compound **13** as a dark purple solid with a yield of 87%. $^1$H NMR (400 MHz, $CDCl_3$) $\delta$ (ppm): 9.20 (s, 2H), 7.32 (s, 2H), 4.05 (d, $J$ = 8.0 Hz, 4H), 1.95 (m, 2H), 1.41−0.92 (m, 96H), 0.87 (m, 12H). $^{13}$C NMR (100 MHz, $CDCl_3$) $\delta$ (ppm): 160.70, 141.78, 140.23, 140.03, 130.09, 126.06, 122.26, 118.89, 108.50, 46.54, 37.77, 31.94, 31.17, 30.02, 29.73, 29.68, 29.59, 29.39, 26.15, 22.71, 14.15. Anal. Calcd for $C_{74}H_{118}Br_2N_2O_2S_4$: C, 65.55; H, 8.77; N, 2.07; S, 9.46. Found: C, 65.60; H, 8.81; N, 2.03; S, 9.40%.

*Synthesis of Compound* ***14***. Compound **14** was obtained by following a similar procedure as that for compound **13** but by starting from compound **9** (0.4 g, 0.31 mmol). Compound **14** was obtained as a dark purple solid with a yield of 89%. $^1$H NMR (400 MHz, $CDCl_3$) $\delta$ (ppm): 9.20 (s, 2H), 7.32 (s, 2H), 4.05 (d, $J$ = 8.0 Hz, 4H), 1.95 (m, 2H), 1.44−0.94 (m, 112H), 0.88 (m, 12H). $^{13}$C NMR (100 MHz, $CDCl_3$) $\delta$ (ppm): 160.69, 141.89, 140.25, 140.07, 130.14, 126.08, 122.30, 119.00, 108.50, 46.58, 37.33, 31.90, 31.18, 29.96, 29.91, 29.89, 29.83, 29.80, 29.55, 29.32, 26.24, 22.85, 22.67, 17.04, 14.12. Anal. Calcd for $C_{82}H_{134}Br_2N_2O_2S_4$: C, 67.09; H, 9.20; N, 1.91; S, 8.74. Found: C, 67.13; H, 9.25; N, 1.86; S, 8.70%.

*Synthesis of Compound* ***15***. Compound **15** was obtained by following a similar procedure as that for compound **13** but by starting


DOI: 10.1021/am508026s
ACS Appl. Mater. Interfaces 2015, 7, 3280−3288

**Scheme 1. Synthesis of PDPPTT-T Polymers Bearing Different Branched Alkyl Side Chains**

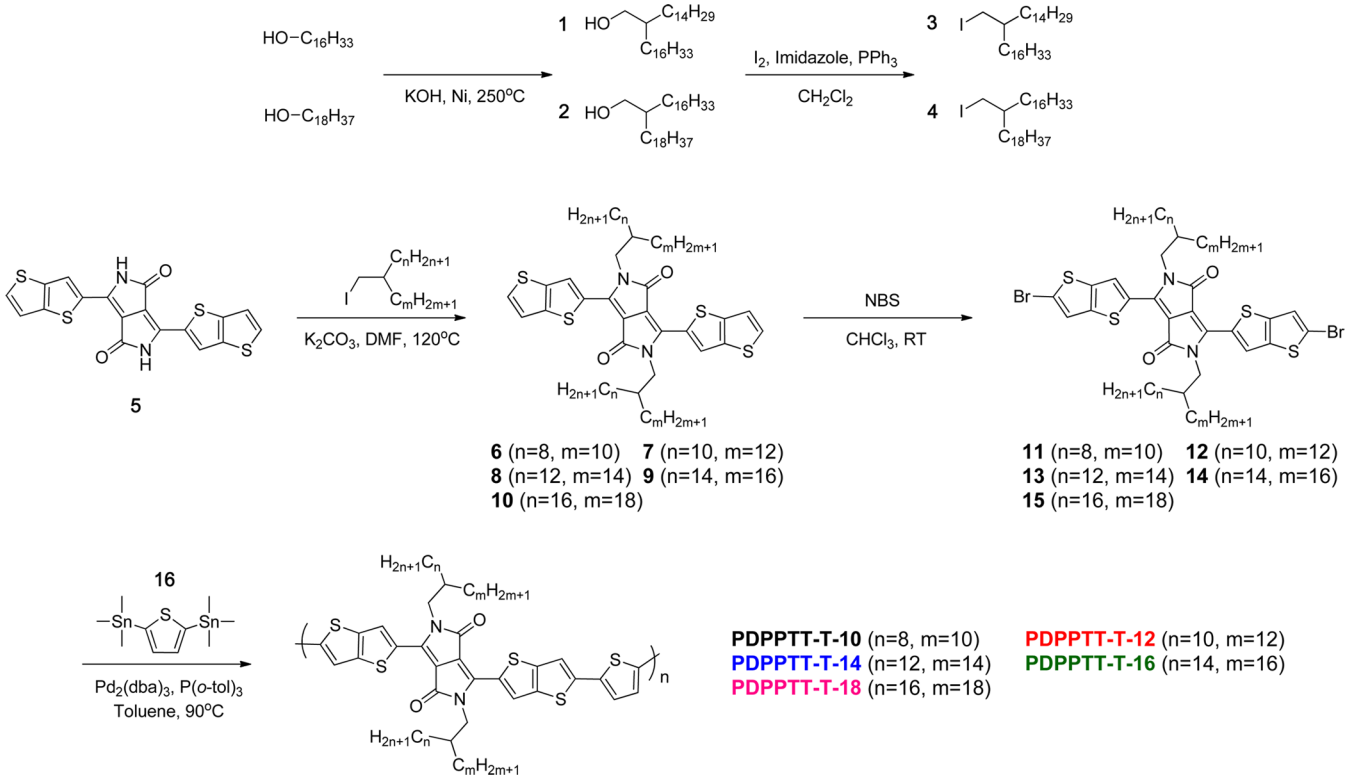


from compound **10** (0.4 g, 0.28 mmol). Compound **15** was obtained as a dark purple solid with a yield of 81%. $^1$H NMR (400 MHz, $CDCl_3$) $\delta$ (ppm): 9.20 (s, 2H), 7.32 (s, 2H), 4.05 (d, $J$ = 8.0 Hz, 4H), 1.95 (m, 2H), 1.47−0.90 (m, 128H), 0.87 (m, 12H). $^{13}$C NMR (100 MHz, $CDCl_3$) $\delta$ (ppm): 160.73, 141.80, 140.24, 140.04, 130.09, 126.04, 122.28, 118.95, 108.52, 46.58, 37.53, 31.91, 31.88, 31.06, 30.15, 30.03, 29.98, 29.92, 29.89, 29.85, 29.57, 29.46, 29.46, 29.37, 26.47, 26.02, 22.75, 22.73, 17.03, 14.25, 14.14. Anal. Calcd for $C_{90}H_{150}Br_2N_2O_2S_4$: C, 68.41; H, 9.57; N, 1.77; S, 8.12. Found: C, 68.37; H, 9.54; N, 1.79; S, 8.15%.

*Synthesis of* ***PDPPTT-T-14***. Monomer **13** (150 mg, 0.11 mmol) and monomer **16** (45 mg, 0.11 mmol) were dissolved in dry toluene (10 mL) that had been degassed with nitrogen for 0.5 h. Tris(dibenzylideneacetone)dipalladium (0) (2.0 mg, 2 mol %) and tri-*o*-tolylphosphine (2.6 mg, 8 mol %) were then added to the mixture, which was kept at 100 °C for 12 h. After the reaction mixture cooled to room temperature, it was added dropwise into a 10:1 mixture of methanol and 1 M aqueous HCl. The crude polymer was collected by filtration and dried at 40 °C under vacuum for 2 h. The predried polymer was then purified by Soxhlet extraction with methanol, acetone, hexane, and chloroform, sequentially. The product was obtained by precipitation of chloroform fraction in methanol and drying under vacuum for 24 h. **PDPPTT-T-14** as a free-standing film was afforded with a yield of 95% ($M_n$ = 69. 5 kDa, PDI = 2.65). Anal. Calcd for $(C_{78}H_{122}N_2O_2S_5)_n$: C, 73.18; H, 9.61; N, 2.19; S, 12.52. Found: C, 73.21; H, 9.58; N, 2.16; S, 12.58%.

*Synthesis of* ***PDPPTT-T-16***. **PDPPTT-T-16** was obtained by following a similar procedure as that for **PDPPTT-T-14** but by starting from monomer **14** (0.4 g, 0.27 mmol). **PDPPTT-T-16** was obtained as a free-standing film with a yield of 90% ($M_n$ = 75.0 kDa, PDI = 2.15). Anal. Calcd for $(C_{86}H_{138}N_2O_2S_5)_n$: C, 74.19; H, 9.99; N, 2.01; S, 11.51. Found: C, 74.22; H, 10.04; N, 2.06; S, 11.46%.

*Synthesis of* ***PDPPTT-T-18***. **PDPPTT-T-18** was obtained by following a similar procedure as that for **PDPPTT-T-14** but by starting from monomer **15** (0.4 g, 0.25 mmol). **PDPPTT-T-18** was obtained as a free-standing film with a yield of 86% ($M_n$ = 58.7 kDa, PDI = 1.82). Anal. Calcd for $(C_{94}H_{154}N_2O_2S_5)_n$: C, 75.04; H, 10.32; N, 1.86; S, 10.66. Found: C, 75.02; H, 10.38; N, 1.81; S, 10.74%.

**Instrumentation.** $^1$H NMR spectra were recorded using a Varian Mercury 400 MHz spectrometer using deuterated chloroform ($CDCl_3$, Cambridge Isotope Laboratories) with tetramethylsilane as a standard. $^{13}$C NMR spectra were recorded at 100 MHz as a solution in $CDCl_3$ on Varian Inova-500 spectrometer. Thermo Scientific Flash 2000 (Thermo Fisher Scientific) elemental analyzer was employed to determine the content of C, H, N, and S. Polymer molecular weights were determined by gel permeation chromatography (GPC, Waters GPC, Waters 515 pump, Waters 410 RI, 2× PLgel Mixed-B) using a polystyrene standard in chloroform ($T$ = 35 °C) and 1,2,4-trichlorobnezne ($T$ = 150 °C) as the eluents at the Korea Polymer Testing & Research Institute (Koptri, Seoul, Korea).

Absorption spectra for both films and solutions were obtained using a UV−vis absorption spectrophotometer (HP 8453, photodiode array) over a wavelength range of 190−1100 nm. A 0.4 wt % chloroform solution of the pertinent DPPTT-T-based polymer was filtered through an Acrodisc syringe filter (Millipore 0.45 $\mu$m), and the thin film was prepared by spin-coating method on glass substrate.

Oxidation properties were examined by cyclic voltammetry (CV) using an eDAQ EA161 potentiostat. The desired thin film was deposited on a platinum plate using a polymer solution in chloroform, while 0.10 M tetrabutylammonium hexafluorophosphate in dry acetonitrile was selected as the electrolyte. The reference electrode was composed of Ag/AgCl, while the counter electrode was made of a platinum wire with a diameter of 0.5 mm. A scan rate of 5.0 mV s$^{-1}$ was used.

To characterize the polymer surface topography, AFM (Advanced Scanning Probe Microscope, XE-100, psia) was employed. A silicon cantilever was used in tapping mode for all scans. Single-polymer and $PC_{71}BM$ blend films were prepared in the same way as those used in the corresponding device fabrication. Two-dimensional GI-XRD measurements were carried out at the PLS-II 9A ultrasmall angle X-ray scattering beamline of Pohang Accelerator Laboratory ($\lambda$ = 1.116 Å, $2\theta$ = 0°−20°). The scattering vectors $q_{xy}$ and $q_z$ are the components parallel and perpendicular to the film surface, respectively. Single-


DOI: 10.1021/am508026s
ACS Appl. Mater. Interfaces 2015, 7, 3280−3288

**Table 1. Optical and Electrochemical Properties of the PDPPTT-T Polymers**

| | | | absorption spectroscopy (nm) | | | energy level | |
|---|---|---|---|---|---|---|---|
| polymer | $M_n$ (kDa) | PDI | solution | film | $E_g^{opt}$ [b] (eV) | HOMO[c] (eV) | LUMO[d] (eV) |
| PDPPTT-T-10 | 332.5 (39.1)[a] | 13.7 (1.47)[a] | 820, 888 | 821, 886 | 1.39 | 5.16 | 3.77 |
| PDPPTT-T-12 | 562.9 (19.1)[a] | 9.22 (2.43)[a] | 815, 887 | 818, 895 | 1.38 | 5.19 | 3.81 |
| PDPPTT-T-14 | 69.5 | 2.65 | 808, 886 | 819, 886 | 1.39 | 5.18 | 3.79 |
| PDPPTT-T-16 | 75.0 | 2.15 | 807, 884 | 820, 883 | 1.40 | 5.20 | 3.80 |
| PDPPTT-T-18 | 58.7 | 1.82 | 803, 880 | 816, 888 | 1.39 | 5.23 | 3.84 |

[a] $M_n$ and PDI were measured by using high-temperature GPC. [b] Optical bandgap calculated by using the equation $E_g^{opt} = 1240/\lambda_{onset}$. [c] Calculated by using the oxidation potentials in CV. [d] LUMO level was calculated from the HOMO level and optical bandgap of the film.

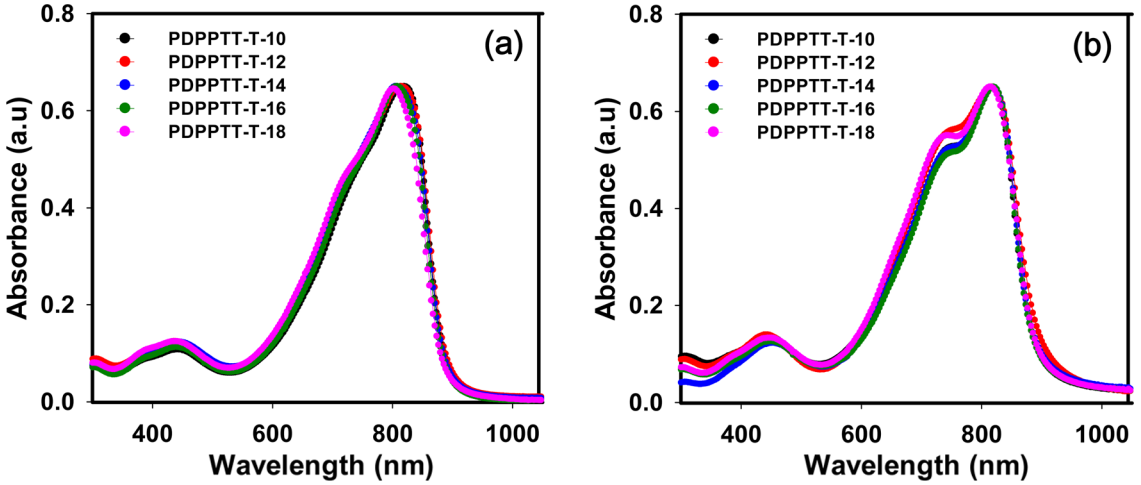


**Figure 1.** UV−vis absorption spectra of the PDPPTT-T polymers (a) in chloroform solution and (b) as pristine films.

polymer and $PC_{71}BM$ blend films were prepared in the same way as those used in the corresponding device fabrication. Grain size was calculated by Scherrer's formula, where $t = (K\lambda/\beta\cos(\theta))$, and $K$ is a constant depending on crystallite shape; $\lambda$ is the X-ray wavelength, $\beta$ is the full width at half-maximum (fwhm), and $\theta$ is the diffraction angle.

**Thin-Film Transistor Device Fabrication and Characterization.** Bottom-gate top-contact TFTs were fabricated on heavily n-doped Si as the gate electrode with $SiO_2$ (300 nm) dielectric layer. *n*-Octyltrichlorosilane (OTS) was used to treat the $SiO_2$ gate dielectric, forming a hydrophobic surface. The polymer film was then deposited on the surface of OTS-treated $SiO_2$ by spin-coating from a chloroform solution (4 mg $mL^{-1}$) at ambient conditions. Finally, the source and drain gold electrodes (thickness = 80 nm) were thermally deposited through a shadow mask under vacuum. Field-effect characteristics of the devices (channel width = 1500 $\mu$m, length = 100 $\mu$m) were determined in air using a Keithley 4200-SCS semiconductor parameter analyzer. Meanwhile, field-effect mobility at saturation ($\mu$) was calculated from the equation $I_{DS} = (W/2L)C_i\mu(V_G - V_{th})^2$, where $W$ and $L$ are the channel width and length, $C_i$ is the gate dielectric layer capacitance per unit area, and $V_G$ and $V_{th}$ are the gate and threshold voltage, respectively.

**Fabrication and Characterization of Polymer Solar Cells.** The indium tin oxide (ITO) glass was first sequentially cleaned in acetone, deionized water, and isopropyl alcohol by sonication, then dried in a vacuum oven for 10 h at 120 °C and treated with $O_2$ plasma (CR403M, 90 W) for 10 min. A 40 nm thick poly(3,4-ethylenedioxythiophene)-poly(styrenesulfonate) (PEDOT:PSS) film (Baytron P) was deposited onto the ITO glass by spin-coating a stock solution of PEDOT:PSS and methanol (2:1, v/v) at 4000 rpm for 40 s. After annealing at 150 °C for 30 min in atmosphere, the substrates were transferred to a glovebox. Solutions of the photoactive layers were prepared by dissolving the appropriate PDPPTT-T polymer and $PC_{71}BM$ (1:2 wt/wt) at a concentration of 20 mg $mL^{-1}$ in a mixed solvent of chloroform and 1,2-dichlorobenzene (4:1, v/v) containing 1 vol % of 1,8-diiodooctane. The blend solution was then spin-coated onto the PEDOT:PSS layer and dried in vacuo.

Electrode fabrication was accomplished by evaporating a 150 nm thick aluminum layer on a LiF thin layer. The active area is 0.04 $cm^2$, and the thickness of the active layer was measured by a Dektak 3 surface profilometer. The current−voltage characteristics were measured with a Keithley 2400 Source Measure Unit. A 300 W Xe lamp was used as a light source, providing an intensity of 100 mW $cm^{-2}$. An AM 1.5 filter (Oriel) and a neutral density filter were used to reduce light intensity when necessary so as to provide a light source that most accurately approximated sunlight. A calibrated broadband optical power meter (Spectra Physics, Model 404) was used for measuring incident light intensity.

## RESULTS AND DISCUSSION

**Synthesis and Properties of DPPTT-Based Polymers.** We employed electron-deficient DPPTT-based monomers as electron acceptors and thiophene monomers as electron donors in constructing the conjugated polymer backbone. The backbone was fixed for all five tested polymers to investigate only the effect of the branched alkyl side chains on polymer properties; the structures and syntheses of these materials are displayed in Scheme 1. **PDPPTT-T-14**, **16**, and **18** had not been previously synthesized, while **PDPPTT-T-10** and **12** were previously reported.[23−25] All polymers were prepared through typical Pd-catalyzed Stille coupling reaction conditions of 100 °C and 12 h and were purified by Soxhlet extraction with methanol, acetone, hexane, and chloroform, sequentially.

All synthesized polymers showed excellent room-temperature solubility in common halogenated organic solvents, specifically chloroform, chlorobenzene, and 1,2-dichlorobenzene. The $M_n$ values of **PDPPTT-T-10**, **PDPPTT-T-12**,


DOI: 10.1021/am508026s
ACS Appl. Mater. Interfaces 2015, 7, 3280−3288

**PDPPTT-T-14**, **PDPPTT-T-16**, and **PDPPTT-T-18** were 332.5, 562.9, 69.5, 75.0, and 58.7 kDa in the chloroform, respectively. (Figure S1, Supporting Information) These, along with PDI values, are displayed in Table 1. Among them, **PDPPTT-T-10** and **PDPPTT-T-12** showed unusually high PDI values; therefore, the $M_n$ and PDI of these polymers were measured through high-temperature GPC using 1,2,4-trichlorobenzene as the eluent and also shown in Table 1. In particular, **PDPPTT-T-14**, **PDPPTT-T-16**, and **PDPPTT-T-18**, all of which contained relatively long and bulky side chains, showed better solubility.

**Optical and Electrochemical Properties.** Figure 1 displayed UV−vis absorption spectra of the five polymers in solution and film states; the resulting parameters are listed in Table 1. The solution spectra showed similar characteristic absorption bands in the range of 600−900 nm, meaning that differences in side-chain composition do not affect photophysical properties in solution (Figure 1a). In contrast, the maximum absorption peak in the thin-film samples was red-shifted slightly and showed a more predominant shoulder peak at ∼740 nm, indicating enhanced intermolecular interaction between the polymer backbones (Figure 1b). Only **PDPPTT-T-10** showed effectively identical spectra between the two states, with maximum absorption values of 820 and 821 nm; this suggests that the polymer chains of **PDPPTT-T-10** were preorganized due to strong intermolecular interaction. However, both **PDPPTT-T-16** and **PDPPTT-T-18** showed differences of ∼13 nm between the maximum absorption peaks of their solution and film spectra, suggesting low interaction in solution due to chain length and branching.

The electrochemical properties of the thin films were measured by CV to evaluate electronic energy levels; results are summarized in Table 1. The highest occupied molecular orbital (HOMO) level tends to decrease with side-chain length and bulkiness; for example, $E_{HOMO}$ = −5.16 and −5.23 eV for **PDPPTT-T-10** and **PDPPTT-T-18**, respectively. This indicates that the steric hindrance of bulkier side chains disrupts conjugation along the polymer backbone, slightly weakening the electron-donating effect. However, while the HOMO levels of the five polymers are slightly different, the optical bandgaps remain relatively similar.

**Characterization of Thin-Film Transistor Device Performance.** The effects of the bulky side chains on the charge-transport properties of the synthesized polymers were investigated by fabricating TFTs. The side chains were found to modulate $\pi-\pi$ stacking distance between the polymer backbones, which can help to increase charge-carrier mobilities and induce dense molecular packing. Under the strategy mentioned above, we fabricated top-contact and bottom-gate TFTs by spin-coating polymer solutions onto OTS-treated substrates and the as-spun films were employed without thermal treatment in TFTs. The fabricated TFT devices were characterized under ambient conditions, with all devices exhibiting typical p-type transistor behavior characterized by high current on/off ratios of $1 \times 10^6$ to $1 \times 10^7$ (Figure 2a). As shown in Table 2, hole mobilities were measured at 1.23 $cm^2 V^{-1} s^{-1}$ for **PDPPTT-T-10**, 0.16 $cm^2 V^{-1} s^{-1}$ for **PDPPTT-T-12**, 1.92 $cm^2 V^{-1} s^{-1}$ for **PDPPTT-T-14**, 0.35 $cm^2 V^{-1} s^{-1}$ for **PDPPTT-T-16**, and 0.14 $cm^2 V^{-1} s^{-1}$ for **PDPPTT-T-18**. This shows that shorter alkyl side chains give higher hole mobilities, while longer alkyl chains perform more poorly. There is an exception to the general trend; PDPPTT-T-12 has a lower hole mobility, which might be ascribed to the unfavorable internal

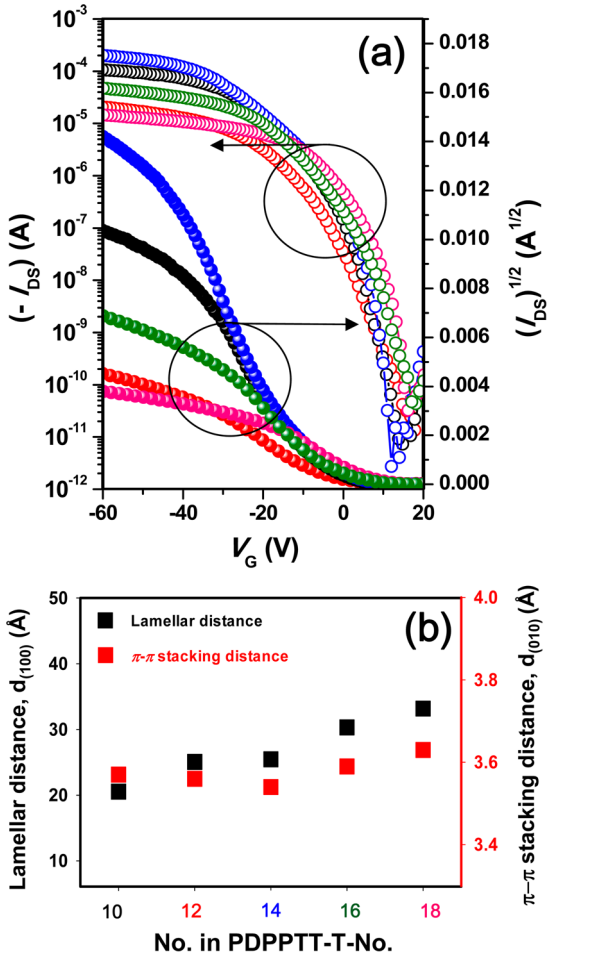


**Figure 2.** (a) Transfer characteristics of PDPPTT-T TFT devices at $V_{DS}$ = −100 V ($L$ = 100 $\mu$m, $W$ = 1500 $\mu$m); Black: PDPPTT-T-10 (linear $V_G$ range: −28 to −19 V); Red: PDPPTT-T-12 (linear $V_G$ range: −26 to −13 V); Blue: PDPPTT-T-14 (linear $V_G$ range: −36 to −21 V); Green: PDPPTT-T-16 (linear $V_G$ range: −27 to −11 V); Pink: PDPPTT-T-18 (linear $V_G$ range: −18 to −2 V). (b) GI-XRD data for the PDPPTT-T polymer films.

morphology and chain arrangement on the substrates. It will be discussed further using the data of GI-XRD and AFM image analysis.

GI-XRD was employed to investigate film crystallinity and polymer chain arrangement on the substrate to better understand the relationship between side-chain bulkiness and TFT charge transport; the same films that were used for the TFT devices were tested here (Figure 3a−e). The polymers all showed (100) and (010) diffraction patterns, which are due to periodic lamellar packing and $\pi-\pi$ stacking of polymer chains in the out-of-plane profiles, respectively. **PDPPTT-T-10** and **PDPPTT-T-14** showed fourth-ordered ($h$00) diffraction peaks (Figure 3), which resulted in fairly well-ordered crystalline lamellar structures built off of the substrate. In addition, the two polymers exhibited relatively strong (010) diffraction peaks at ∼17.9−18.1°. Therefore, they showed a dominant edge-on orientation over face-on orientation, while the others showed a face-on orientation predominantly with respect to the substrate. In particular, **PDPPTT-T-12**, **PDPPTT-T-16**, and **PDPPTT-T-18** exhibited stronger in-plane diffraction peaks of ($h$00), which are comparable to those in the out-of-plane profiles, as shown in Figure 3b,g,h. The $\pi-\pi$ stacking distance of


DOI: 10.1021/am508026s
ACS Appl. Mater. Interfaces 2015, 7, 3280−3288

**Table 2. TFT and PSC Characteristics of the PDPPTT-T Polymers**

| polymer | $I_{on}/I_{off}$ | $V_{th}$ (V) | $\mu$ ($cm^2\ V^{-1}\ s^{-1}$)[a] | $V_{oc}$ (V) | $J_{sc}$ ($mA/cm^2$) | FF | PCE[b] (%) | thickness[c] (nm) |
|---|---|---|---|---|---|---|---|---|
| PDPPTT-T-10 | $1 \times 10^7$ | −5.0 | 1.23 (1.15) | 0.60 | −17.26 | 0.56 | 5.79 (5.60) | 171 |
| PDPPTT-T-12 | $1 \times 10^6$ | −2.0 | 0.16 (0.10) | 0.62 | −15.02 | 0.53 | 4.93 (4.71) | 168 |
| PDPPTT-T-14 | $1 \times 10^7$ | −6.0 | 1.92 (1.78) | 0.60 | −7.20 | 0.50 | 2.16 (2.14) | 166 |
| PDPPTT-T-16 | $1 \times 10^6$ | −0.5 | 0.36 (0.32) | 0.60 | −4.68 | 0.45 | 1.26 (1.20) | 161 |
| PDPPTT-T-18 | $1 \times 10^5$ | 5.0 | 0.14 (0.12) | 0.60 | −3.81 | 0.34 | 0.78 (0.71) | 157 |

[a]Unannealed film. [b]Optimized devices with a polymer/$PC_{71}BM$ ratio of 1:2 (w/w) with DIO (1%) additive. [c]The average thickness of active layer for OPVs. $\mu$ ($cm^2\ V^{-1}\ s^{-1}$), $I_{on}/I_{off}$ and $V_{th}$ (V) are the hole mobility, the current on/off ratio, and the threshold voltage, respectively. $J_{sc}$ ($mA/cm^2$) is the short-circuit current density, $V_{oc}$ (V) is the open circuit voltage, FF is the fill factor, PCE (%) is the power conversion efficiency. Average mobilities and power conversion efficiencies are in parentheses for >20 devices.

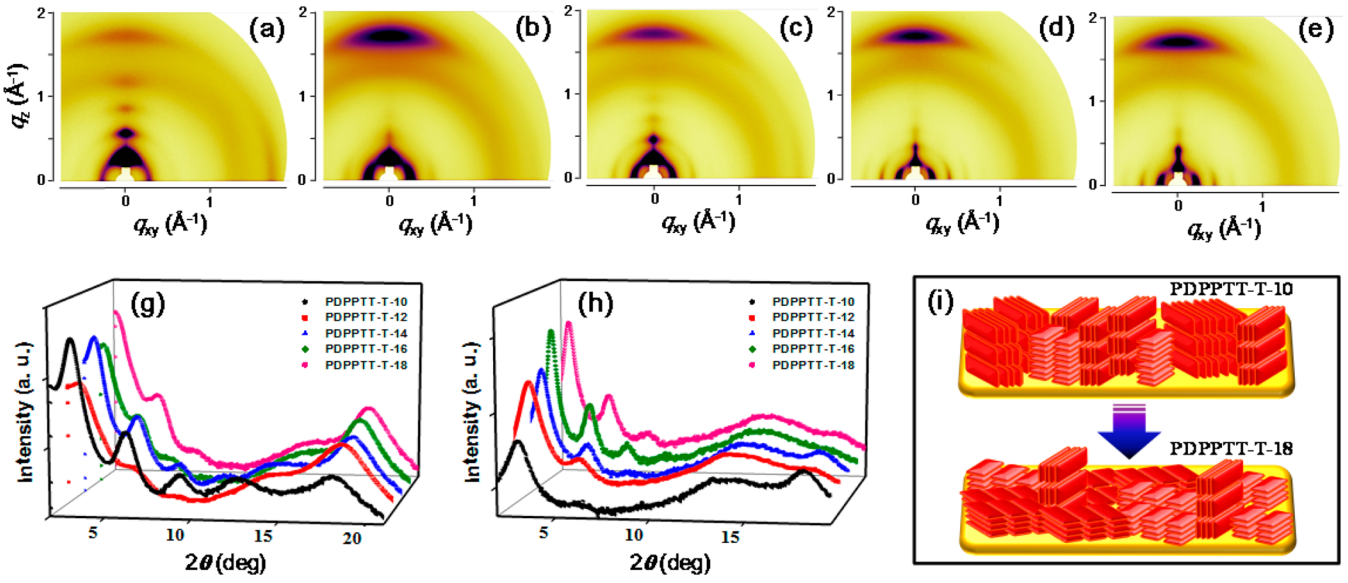


**Figure 3.** Two-dimensional GI-XRD patterns of (a) PDPPTT-T-10, (b) PDPPTT-T-12, (c) PDPPTT-T-14, (d) PDPPTT-T-16, and (e) PDPPTT-T-18. (g, h) Out-of-plane and in-plane profiles, respectively. (i) Schematic packing diagrams of the polymer chains on the substrates.

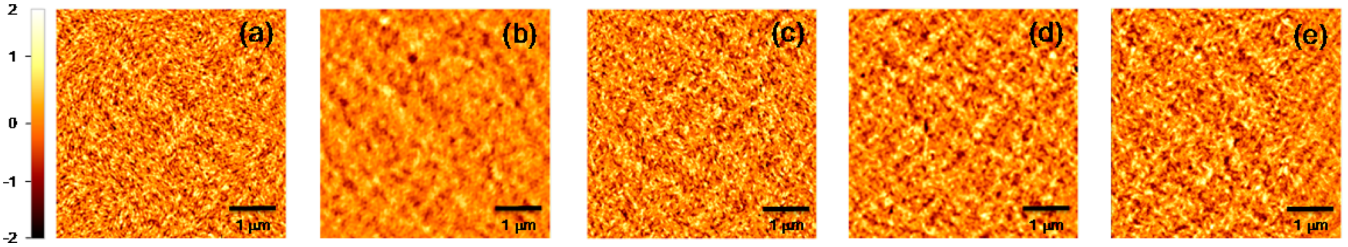


**Figure 4.** AFM height images (5 $\mu$m × 5 $\mu$m) of (a) PDPPTT-T-10, (b) PDPPTT-T-12, (c) PDPPTT-T-14, (d) PDPPTT-T-16, and (e) PDPPTT-T-18 polymer films.

**PDPPTT-T-14** was calculated to be the smallest, as shown in Figure 2b, which indicates that the polymer can affect more efficient charge transport to a small extent. On the other hand, highly resolved lamellar diffraction and negligible (010) diffraction peaks were observed for **PDPPTT-T-12**, **PDPPTT-T-16**, and **PDPPTT-T-18** in plane-profiles, which resulted in lower charge-carrier mobilities.

AFM was employed to investigate the surface topography of the thin films, as this feature contributes significantly to TFT performance. All polymer films were relatively smooth, with roughness values of less than 2 nm (Figure 4). The surfaces of **PDPPTT-T-10** and **PDPPTT-T-14** were filled with relatively fine domains, while those of **PDPPTT-T-12**, **PDPPTT-T-16**, and **PDPPTT-T-18** were less dense, further supporting the conclusion that **PDPPTT-T-10** and **PDPPTT-T-14** displayed higher charge-carrier mobility.

**Polymer Solar Cell Performance and Characterization of the Blend Films.** To optimize device performances of PDPPTT-T based solar cells, various devices were fabricated with the kind of solvent and acceptor molecules. (Figures S2–S6, Supporting Information) Eventually, alkyl side-chain effects on PSC performance were investigated by fabricating bulk heterojunction devices with a standard ITO/PEDOT:PSS/PDPPTT-T:$PC_{71}BM$/LiF/Al configuration. The solar cell photoactive layers were fabricated using the same PDPPTT-T/$PC_{71}BM$ = 1:2 (w/w) blend ratio and 20 mg $mL^{-1}$ solution concentration so as to control for all potential variables. Device performance was measured under 100 $mW/cm^2$ AM 1.5 G illumination.


DOI: 10.1021/am508026s
ACS Appl. Mater. Interfaces 2015, 7, 3280–3288

Figure 5 shows the current density−voltage ($J$−$V$) curves of the **PDPPTT-T**-based PSCs, while device performance is

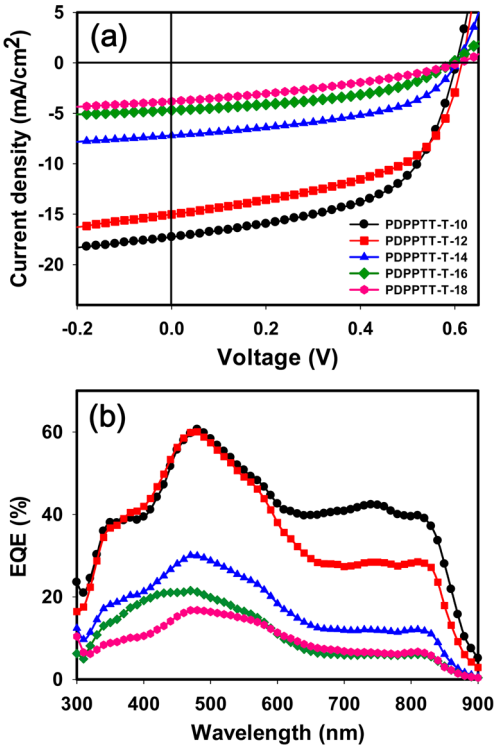


**Figure 5.** (a) $J$−$V$ characteristics and (b) EQE spectra of the PDPPTT-T polymer/$PC_{71}BM$ devices.

summarized in Table 2. All devices showed similar open-circuit voltages, an observation that is supported by the similar HOMO levels determined by CV. Meanwhile, short-circuit current density ($J_{sc}$), PCE, and the fill factor (FF) were found to decrease as side chain size increased. **PDPPTT-T-10** exhibited the highest $J_{sc}$ of 17.26 mA $cm^{-2}$, giving a PCE of 5.79%, whereas **PDPPTT-T-14** gave a $J_{sc}$ of 7.20 mA $cm^{-2}$, resulting in a lower PCE of 2.16% despite the higher carrier mobility observed in the TFT. In contrast, **PDPPTT-T-12**, with its lower $M_n$, exhibited much better device performance, with a $J_{sc}$ of 15.02 mA $cm^{-2}$ and a PCE of 4.93%.

The external quantum efficiency (EQE) spectra of the PSC devices are shown in Figure 5b; all five polymers exhibited broad and highly efficient light-harvesting, ranging from 300 to 900 nm in the visible and near-infrared wavelength. The **PDPPTT-T-10** device in particular showed EQE values that were consistent with the fact that it had the highest $J_{sc}$ in the $J$−$V$ analysis. This can be attributed to greater miscibility, leading to the formation of nanophase-separated domains between the polymer and $PC_{71}BM$ crystallites/crystallite aggregates.

The surface morphology of the active PSC layer was measured by AFM to better understand the basis for the improved performance observed. As shown in Figure 6, the **PDPPTT-T-10**:$PC_{71}BM$ blended film showed very fine surface morphology, with a root-mean-square roughness of 2.5 nm; such a quality might be favorable for exciton generation and migration through nanoscopically separated domains, thereby contributing significantly to the higher $J_{sc}$ value observed. Compared to the surface morphological textures of **PDPPTT-T-10** and **PDPPTT-T-12**, **PDPPTT-T-14**, **PDPPTT-T-16**, and **PDPPTT-T-18** exhibited much coarser texture and large phase separation between polymer and $PC_{71}BM$ crystallites, which results in poor PCEs.

GI-XRD patterns of the PDPPTT-T:$PC_{71}BM$ blended films were analyzed to expand on the conclusions drawn from the AFM data (Figure 7a−e). The ($h$00) diffraction patterns were clearer in the out-of-plane profile as the bulkiness of the alkyl side chains increased. In the in-plane profiles, the blend films did not exhibit significant difference except for **PDPPTT-T-18**. This suggests that increased bulkiness resulted in poor miscibility between the polymers and $PC_{71}BM$, leading to microphase-separated domains that reduced exciton diffusion and yielded decreasing $J_{sc}$ values. (Figure 7f,g) The surface roughness observed by AFM analysis showed same tendency with the $\pi$−$\pi$ stacking distance between the polymer backbones. In addition, the $\pi$−$\pi$ stacking distance decreased throughout when bulkiness decreased (Figure 7h). **PDPPTT-T-10** had the smallest $\pi$−$\pi$ stacking distance ($d_{(010)}$ = 3.54 Å) as well as the smallest grain size calculated with fwhm of $d_{(100)}$ peak, which can contribute to increased $J_{sc}$ values, and, consequently, improved PCE (Figure 7i). In Figure 7j, the schematic images of internal morphology of blend films with **PDPPTT-T-10** and **PDPPTT-T-18** were illustrated for comparison. In brief, increased bulkiness of the side chain reduces $J_{sc}$ and FF due to the resulting increased domain size and surface roughness; these factors elicit poor exciton diffusion and poor charge separation, which in turn induce charge recombination and a corresponding reduction in PSC device performance.[27−29]

## CONCLUSIONS

We systematically designed and synthesized new DPPTT- and thiophene-containing $\pi$-extended conjugated polymers bearing 2-octyldodecyl, 2-decyltetradecyl, 2-tetradecylhexadecyl, 2-hexadecyloctadecyl, and 2-octadecyldocosyl bulky branched alkyl side chains tethered to the N-positions of the thienothiophene-flanked diketopyrrolopyrrole unit. All five conjugated polymers were soluble due to the side-chain

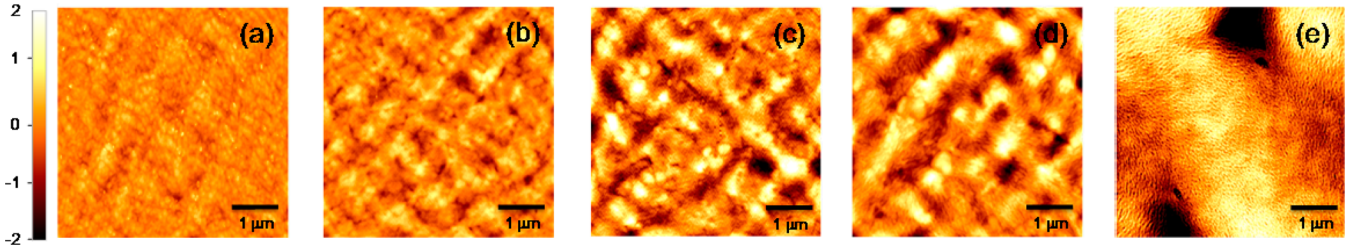


**Figure 6.** AFM height images (5 $\mu$m × 5 $\mu$m) of (a) PDPPTT-T-10, (b) PDPPTT-T-12, (c) PDPPTT-T-14, (d) PDPPTT-T-16, and (e) PDPPTT-T-18 blended films with $PC_{71}BM$.


DOI: 10.1021/am508026s
ACS Appl. Mater. Interfaces 2015, 7, 3280−3288

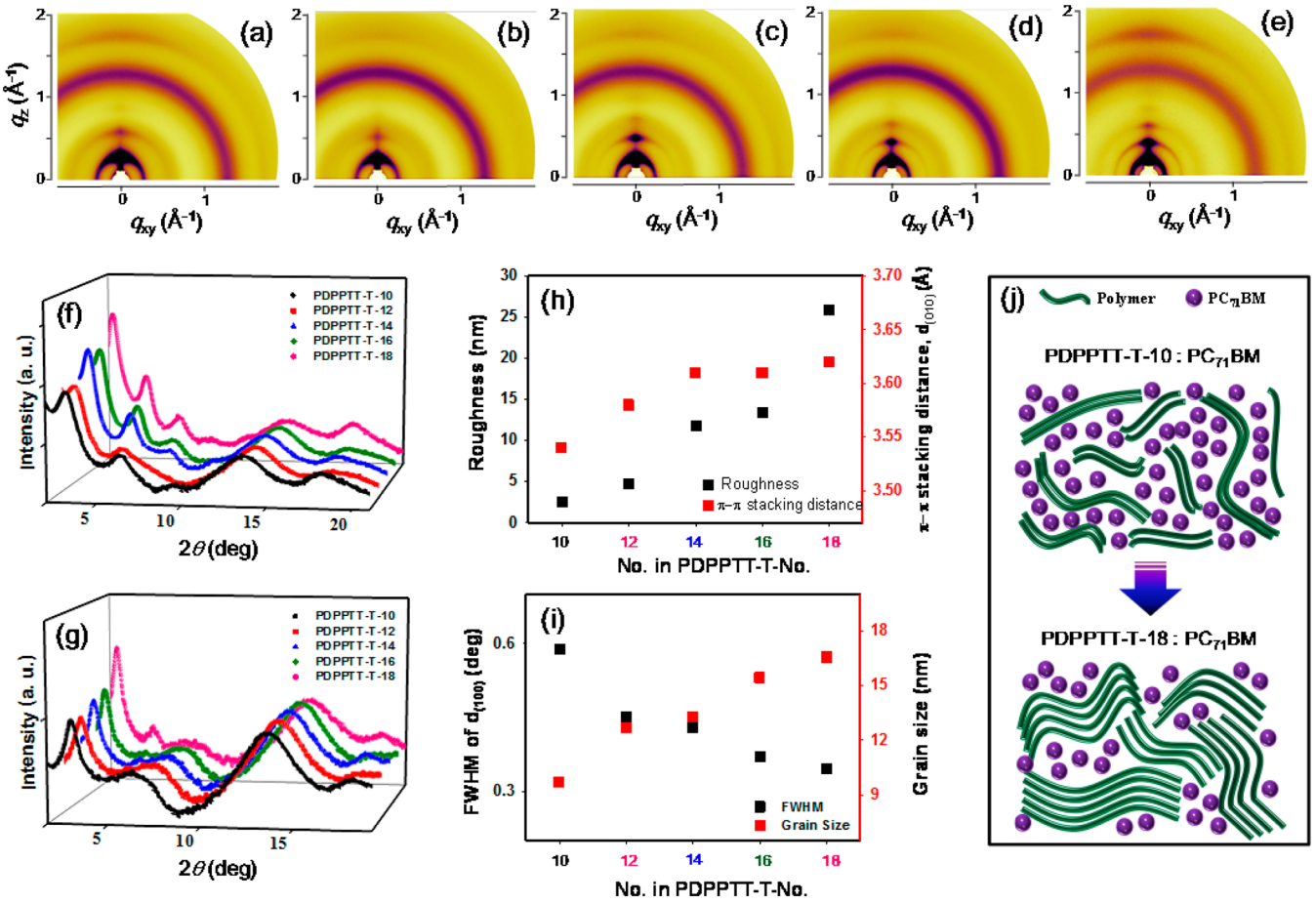


**Figure 7.** Two-dimensional GI-XRD patterns of (a) PDPPTT-T-10, (b) PDPPTT-T-12, (c) PDPPTT-T-14, (d) PDPPTT-T-16, and (e) PDPPTT-T-18 blended films with $PC_{71}BM$. (f) Out-of-plane and (g) in-plane profiles. (h, i) Roughness and GI-XRD data for the blended films. (j) A schematic of the blended film morphology.

bulkiness. The **PDPPTT-T-14**-based TFT had the highest hole mobility of 1.92 $cm^2$ $V^{-1}$ $s^{-1}$, the result of having the smallest $\pi-\pi$ stacking distance. Meanwhile, the **PDPPTT-T-10** device showed the highest PCE of 5.8% when integrated into heterojunction-type PSCs and mixed with $PC_{71}BM$. The alkyl side chains in the conjugated polymer backbone play important roles to improve solubility and to vary solid-state morphology. Although there is no absolute rule in side-chain engineering, the size of alkyl side chain should be optimized to give high performance of electronic and optoelectronic devices.

## ■ ASSOCIATED CONTENT

### Ⓢ Supporting Information

GPC chromatograms of the five polymers and photovoltaic performances obtained under different processing conditions. This material is available free of charge via the Internet at http://pubs.acs.org.

## ■ AUTHOR INFORMATION

### Corresponding Author

*E-mail: dhchoi8803@korea.ac.kr.

### Notes

The authors declare no competing financial interest.

## ■ ACKNOWLEDGMENTS

This research was supported by National Research Foundation of Korea (NRF2012R1A2A1A01008797) and by Key Research Institute Program (NRF20100020209). We are grateful to Pohang Accelerator Laboratory (Pohang, Korea) for allowing us to conduct the grazing incidence X-ray diffraction (GI-XRD) measurements.

## ■ REFERENCES

(1) Facchetti, A. $\pi$-Conjugated Polymers for Organic Electronics and Photovoltaic Cell Applications. *Chem. Mater.* **2010**, *23*, 733−758.

(2) Helgesen, M.; Søndergaard, R.; Krebs, F. C. Advanced Materials and Processes for Polymer Solar Cell Devices. *J. Mater. Chem.* **2010**, *20*, 36−60.

(3) Biniek, L.; Schroeder, B. C.; Nielsen, C. B.; McCulloch, I. Recent Advances in High Mobility Donor−Acceptor Semiconducting Polymers. *J. Mater. Chem.* **2012**, *22*, 14803−14813.

(4) Sun, B.; Hong, W.; Yan, Z.; Aziz, H.; Li, Y. Record High Electron Mobility of 6.3 $cm^2$ $V^{-1}$ $s^{-1}$ Achieved for Polymer Semiconductors Using a New Building Block. *Adv. Mater.* **2014**, *26*, 2636−2642.

(5) Kang, I.; Yun, H.-J.; Chung, D. S.; Kwon, S.-K.; Kim, Y.-H. Record High Hole Mobility in Polymer Semiconductors via Side-Chain Engineering. *J. Am. Chem. Soc.* **2013**, *135*, 14896−14899.

(6) Lee, J.; Chung, J. W.; Jang, J.; Kim, D. H.; Park, J.-I.; Lee, E.; Lee, B.-L.; Kim, J.-Y.; Jung, J. Y.; Park, J. S.; Koo, B.; Jin, Y. W.; Kim, D. H. Influence of Alkyl Side Chain on the Crystallinity and Trap Density of States in Thiophene and Thiazole Semiconducting Copolymer Based Inkjet-Printed Field-Effect Transistors. *Chem. Mater.* **2013**, *25*, 1927−1934.

(7) Yang, L.; Zhou, H.; You, W. Quantitatively Analyzing the Influence of Side Chains on Photovoltaic Properties of Polymer-Fullerene Solar Cells. *J. Phys. Chem. C* **2010**, *114*, 16793−16800.



DOI: 10.1021/am508026s
*ACS Appl. Mater. Interfaces* 2015, 7, 3280−3288

(8) Li, Y.; Chen, Y.; Liu, X.; Wang, Z.; Yang, X.; Tu, Y.; Zhu, X. Controlling Blend Film Morphology by Varying Alkyl Side Chain in Highly Coplanar Donor-Acceptor Copolymers for Photovoltaic Application. *Macromolecules* **2011**, *44*, 6370−6381.
(9) Bronstein, H.; Leem, D. S.; Hamilton, R.; Woebkenberg, P.; King, S.; Zhang, W.; Ashraf, R. S.; Heeney, M.; Anthopoulos, T. D.; Mello, J. d.; McCulloch, I. Indacenodithiophene-co-benzothiadiazole Copolymers for High Performance Solar Cells or Transistors via Alkyl Chain Optimization. *Macromolecules* **2011**, *44*, 6649−6652.
(10) Deng, Y.; Chen, Y.; Liu, J.; Liu, L.; Tian, H.; Xie, Z.; Geng, Y.; Wang, F. Low-Band-Gap Conjugated Polymers of Dithieno[2,3-b:7,6-b]carbazole and Diketopyrrolopyrrole: Effect of the Alkyl Side Chain on Photovoltaic Properties. *ACS Appl. Mater. Interfaces* **2013**, *5*, 5741−5747.
(11) Yiu, A. T.; Beaujuge, P. M.; Lee, O. P.; Woo, C. H.; Toney, M. F.; Fréchet, J. M. J Side-Chain Tunability of Furan-Containing Low-Band-Gap Polymers Provides Control of Structural Order in Efficient Solar Cells. *J. Am. Chem. Soc.* **2012**, *134*, 2180−2185.
(12) Wang, Y.; Xin, X.; Lu, Y.; Xiao, T.; Xu, X.; Zhao, N.; Hu, X.; Ong, B. S.; Ng, S. C. Substituent Effects on Physical and Photovoltaic Properties of 5,6-Difluorobenzo[c][1,2,5]thiadiazole-Based D−A Polymers: Toward a Donor Design for High Performance Polymer Solar Cells. *Macromolecules* **2013**, *46*, 9587−9592.
(13) Mcculloch, I.; Heeney, M.; Bailey, C.; Genevicius, K.; Macdonald, I.; Shkunov, M.; Sparrowe, D.; Tierney, S.; Wagner, R.; Zhang, W.; Chabinyc, M. L.; Kline, R. J.; McGehee, M. D.; Toney, M. F. Liquid-Crystalline Semiconducting Polymers with High Charge-Carrier Mobility. *Nat. Mater.* **2006**, *5*, 328−333.
(14) Mei, J.; Bao, Z. Side Chain Engineering in Solution-Processable Conjugated Polymers. *Chem. Mater.* **2014**, *26*, 604−615.
(15) Li, Y.; Singh, S. P.; Sonar, P. A High Mobility P-Type DPP-Thieno[3,2- b ]thiophene Copolymer for Organic Thin-Film Transistors. *Adv. Mater.* **2010**, *22*, 4862−4866.
(16) Subramaniyan, S.; Xin, H.; Kim, F. S.; Shoaee, S.; Durrant, J. R.; Jenekhe, S. A. Effects of Side Chains on Thiazolothiazole-Based Copolymer Semiconductors for High Performance Solar Cells. *Adv. Mater.* **2011**, *1*, 854−860.
(17) Lei, T.; Dou, J.-H.; Pei, J. Influence of Alkyl Chain Branching Positions on the Hole Mobilities of Polymer Thin-Film Transistors. *Adv. Mater.* **2012**, *24*, 6457−6461.
(18) Wang, B.; Zhang, J.; Tam, H. L.; Wu, B.; Zhang, W.; Chan, M. S.; Pan, F.; Yu, G.; Zhu, F.; Wong, M. S. Impact of Alkyl Side Chains on the Photovoltaic and Charge Mobility Properties of Naphthodithiophene−Benzothiadiazole Copolymers. *Polym. Chem.* **2014**, *5*, 836−843.
(19) Warnan, J.; Cabanetos, C.; Bude, R.; Labban, A. E.; Li, L.; Beaujuge, P. M. Electron-Deficient N-Alkyloyl Derivatives of Thieno-[3,4-c]pyrrole-4,6-dione Yield Efficient Polymer Solar Cells with Open-Circuit Voltages > 1 V. *Chem. Mater.* **2014**, *26*, 2829−2835.
(20) Son, H. J.; Lu, L.; Chen, W.; Xu, T.; Zheng, T.; Carsten, B.; Strzalka, J.; Darling, S. B.; Chen, L. X.; Yu, L. Synthesis and Photovoltaic Effect in Dithieno[2,3- d:2′, 3′ - d′ ]Benzo[1,2- b:4,5- b′ ]dithiophene-Based Conjugated Polymers. *Adv. Mater.* **2013**, *25*, 838−843.
(21) Meager, I.; Ashraf, R. S.; Mollinger, S.; Schroeder, B. C.; Bronstein, H.; Beatrup, D.; Vezie, M. S.; Kirchartz, T.; Salleo, A.; Nelson, J.; McCulloch, I. Photocurrent Enhancement from Diketopyrrolopyrrole Polymer Solar Cells through Alkyl-Chain Branching Point Manipulation. *J. Am. Chem. Soc.* **2013**, *135*, 11537−11540.
(22) Graham, K. R.; Cabanetos, C.; Jahnke, J. P.; Idso, M. N.; Labban, A. E.; Ndjawa, G. O. N.; Heumueller, T.; Vandewal, K.; Salleo, A.; Chmelka, B. F.; Amassian, A.; Beaujuge, P. M.; McGehee, M. D. Importance of the Donor:Fullerene Intermolecular Arrangement for High-Efficiency Organic Photovoltaics. *J. Am. Chem. Soc.* **2014**, *136*, 9608−9618.
(23) Bronstein, H.; Chen, Z.; Ashraf, R. S.; Zhang, W.; Du, J.; Durrant, J. R.; Tuladhar, P. S.; Song, K.; Watkins, S. E.; Geerts, Y.; Wienk, M. M.; Janssen, R. A. J.; Anthopoulos, T.; Sirringhaus, H.; Heeney, M.; McCulloch, I. Thieno[3,2-b]thiophene-Diketopyrrolopyrrole-Containing Polymers for High-Performance Organic Field-Effect Transistors and Organic Photovoltaic Devices. *J. Am. Chem. Soc.* **2011**, *133*, 3272−3275.
(24) Bronstein, H.; Collado-Fregoso, E.; Hadipour, A.; Soon, Y. W.; Huang, Z.; Dimitrov, S. D.; Ashraf, R. S.; Rand, B. P.; Watkins, S. E.; Tuladhar, P. S.; Meager, I.; Durrant, J. R.; McCulloch, I. Thieno[3,2- b ]thiophene-diketopyrrolopyrrole Containing Polymers for Inverted Solar Cells Devices with High Short Circuit Currents. *Adv. Funct. Mater.* **2013**, *23*, 5647−5654.
(25) Meager, I.; Ashraf, R. S.; Rossbauer, S.; Bronstein, H.; Donaghey, J. E.; Marshall, J.; Schroeder, B. C.; Heeney, M.; Anthopoulos, T. D.; McCulloch, I. Alkyl Chain Extension as a Route to Novel Thieno[3,2-b]thiophene Flanked Diketopyrrolopyrrole Polymers for Use in Organic Solar Cells and Field Effect Transistors. *Macromolecules* **2013**, *46*, 5961−5967.
(26) Heinrich, A. C. J.; Thiedemann, B.; Gates, P. J.; Staubitz, A. Dual Selectivity: Electrophile and Nucleophile Selective Cross-Coupling Reactions on a Single Aromatic Substrate. *Org. Lett.* **2013**, *15*, 4666−4669.
(27) Zhou, H.; Yang, L.; Xiao, S.; Liu, S.; You, W. Donor-Acceptor Polymers Incorporating Alkylated Dithienylbenzothiadiazole for Bulk Heterojunction Solar Cells: Pronounced Effect of Positioning Alkyl Chains. *Macromolecules* **2010**, *43*, 811−820.
(28) Song, H.-J.; Kim, D.-H.; Lee, E.-J.; Heo, S.-W.; Lee, J.-Y.; Moon, D.-K. Conjugated Polymer Consisting of Quinacridone and Benzothiadiazole as Donor Materials for Organic Photovoltaics: Coplanar Property of Polymer Backbone. *Macromolecules* **2012**, *45*, 7815−7822.
(29) Egbe, D. A. M.; Tüurk, S.; Rathgeber, S.; Küuhnlenz, F.; Jadhav, R.; Wild, A.; Birckner, E.; Adam, G.; Pivrikas, A.; Cimrova, V.; Knör, G.; Sariciftci, N. S.; Hoppe, H. Anthracene Based Conjugated Polymers: Correlation between $\pi$-$\pi$-Stacking Ability, Photophysical Properties, Charge Carrier Mobility, and Photovoltaic Performance. *Macromolecules* **2010**, *43*, 1261−1269.


DOI: 10.1021/am508026s
*ACS Appl. Mater. Interfaces* 2015, 7, 3280−3288